High-resolution storage-ring measurements of the dissociative recombination of H_3^+ using a supersonic expansion ion source

Holger Kreckel,[1,*] Oldřich Novotný,[2] Kyle N. Crabtree,[1] Henrik Buhr,[4,3] Annemieke Petrignani,[3] Brian A. Tom,[1,†] Richard D. Thomas,[5] Max H. Berg,[3] Dennis Bing,[3] Manfred Grieser,[3] Claude Krantz,[3] Michael Lestinsky,[2] Mario B. Mendes,[3] Christian Nordhorn,[3] Roland Repnow,[3] Julia Stützel,[3] Andreas Wolf,[3] and Benjamin J. McCall[1,6]

[1]*Department of Chemistry, University of Illinois at Urbana-Champaign, Urbana, Illinois 61801, USA*

[2]*Columbia Astrophysics Laboratory, 550 West 120th Street, New York, New York 10027, USA*

[3]*Max-Planck-Institut für Kernphysik, Saupfercheckweg 1, D-69117 Heidelberg, Germany*

[4]*Faculty of Physics, Weizmann Institute of Science, Rehovot 76100, Israel*

[5]*Department of Physics, Stockholm University, Alba Nova, S-106 91 Stockholm, Sweden*

[6]*Department of Astronomy, University of Illinois at Urbana-Champaign, Urbana, Illinois 61801, USA*

(Received 14 July 2010; published 25 October 2010)

We have performed measurements of the dissociative electron recombination (DR) of H_3^+ at the ion storage ring TSR utilizing a supersonic expansion ion source. The ion source has been characterized by continuous wave cavity ring-down spectroscopy. We present high-resolution DR rate coefficients for different nuclear spin modifications of H_3^+ combined with precise fragment imaging studies of the internal excitation of the H_3^+ ions inside the storage ring. The measurements resolve changes in the energy dependence between the ortho-H_3^+ and para-H_3^+ rate coefficients at low center-of-mass collision energies. Analysis of the imaging data indicates that the stored H_3^+ ions may have higher rotational temperatures than previously assumed, most likely due to collisional heating during the extraction of the ions from the ion source. Simulations of the ion extraction shed light on possible origins of the heating process and how to avoid it in future experiments.

DOI: 10.1103/PhysRevA.82.042715 PACS number(s): 34.80.Ht, 34.80.Lx, 33.20.Ea

I. INTRODUCTION

The dissociative electron recombination (DR) of H_3^+ has received a good deal of attention in recent decades. As it is acknowledged as one of the key reactions of interstellar chemistry [1], many groups around the world have invested considerable effort into the determination of the DR rate coefficient at low temperatures. More than 30 experimental studies of the DR of H_3^+ have been published. It is beyond the scope of this article to list all the references; a review can be found in [2]. In brief, early H_3^+ DR measurements in the seventies resulted in rate coefficients on the order of 10^{-7} cm^3 s^{-1}. In the eighties there was a period of time when the H_3^+ DR reaction was believed to be much slower, based on flowing afterglow experiments giving upper limits for the rate coefficient of 10^{-8} cm^3 s^{-1} [3] and 10^{-11} cm^3 s^{-1} [4]. These conclusions were drawn in accordance with contemporary theory [5], predicting a very small DR rate coefficient. A few years later spectroscopic measurements carried out by Amano [6] and the storage-ring measurements of Larsson *et al.* [7] again supported a faster DR process.

The last decade has seen the storage-ring community striving for better control of the internal temperature of the H_3^+ ions. While it could be shown that the spontaneous decay of vibrationally excited states is fast enough to yield vibrationally cold ions within 2 s of storage [8], it was also found that rotational relaxation proceeds much more slowly [8,9]. In fact, the existence of metastable rotational states of H_3^+ with lifetimes exceeding months [10] makes it impractical to rely on spontaneous decay alone. Therefore, dedicated ion sources that precool the H_3^+ ions prior to injection into the storage ring were employed. McCall *et al.* carried out measurements at CRYRING using a supersonic expansion source for rotational cooling [11,12]. Kreckel *et al.* developed a cryogenic 22-pole ion trap to produce cold ions for DR measurements at TSR [13,14]. Both measurements showed excellent agreement. In the meantime the storage-ring rate coefficient has become the accepted reference.

In order to understand the discrepancies between the storage-ring results and afterglow measurements, detailed studies of hydrogen plasmas have been conducted by Glosík *et al.* [15,16]. They show that at the high pressures necessary to establish a continuous gas flow in afterglow setups, ternary collisions influence the outcome of the measurements. These findings and appropriate corrections may finally remove the disagreements between afterglow and storage-ring experiments [16].

For H_3^+, electron recombination can result in either two or three neutral fragments,

$$H_3^+ + e^- \rightarrow \begin{cases} H(1s) + H(1s) + H(1s), \\ H_2(X^1\Sigma_g^+) + H(1s). \end{cases} \quad (1)$$

While the total rate coefficient is the primary goal of most studies, the branching ratio between the two- and three-body channels has also been determined experimentally [17], as well as the vibrational excitation of the product H_2 molecules in the two-body case and the momentum sharing in the three-body case [9].

On the theoretical frontier a lot of progress has been made in the last decade. Early studies that predicted a very low recombination rate were born in the spirit that a curve crossing between the ionic state and a repulsive neutral state represents

*hkreckel@illinois.edu

†Present address: Department of Chemistry, United States Air Force Academy, CO 80840, USA.

the only effective DR mechanism [5]. This notion has been abandoned and the mechanism driving H_3^+ DR at low energies has been identified [18]. Modern calculations agree well with the storage-ring measurements on the absolute scale of the rate coefficient, while distinct discrepancies still remain for the exact shape of the cross section [19–21].

More recently, storage-ring measurements have been carried out that manipulate the nuclear spin of H_3^+. It has been shown that at low electron energies the rate coefficient of para-H_3^+ is faster than the one for ortho-H_3^+ [13,22] (from here on we will denote ortho-H_3^+ and para-H_3^+ by o-H_3^+ and p-H_3^+, and normal H_2 and para-H_2 by n-H_2 and p-H_2, respectively). Kreckel *et al.* measured the difference of the DR rate coefficient of H_3^+ created from n-H_2 and p-H_2, respectively, using a cryogenic 22-pole trap as an ion injector at TSR [13]. Tom *et al.* used a supersonic expansion ion source that was characterized by cavity ring-down spectroscopy for a DR experiment at CRYRING [22]. Both measurements remain somewhat incomplete, however, since Kreckel *et al.* did not determine the p-H_3^+ fraction, and since both studies are impeded by low electron energy resolution.

In this work we present high-resolution DR measurements with a spectroscopically characterized supersonic expansion ion source using p-H_2 and n-H_2 as a precursor gas. Furthermore, we have carried out DR fragment imaging measurements with this ion source in order to determine the rotational temperature of the H_3^+ ions inside the storage ring.

The paper is organized as follows: the next section gives a brief overview of the storage-ring technique and the supersonic ion source. Section III describes the spectroscopic characterization of the ion source. In Sec. IV the results of the DR rate coefficient and fragment imaging measurements are presented. Section V outlines a possible collisional heating mechanism and in Sec. VI a summary is given and perspectives for future experiments are described.

II. EXPERIMENT

A. Storage-ring technique

The DR measurements were carried out at the TSR storage ring of the Max-Planck-Institut für Kernphysik in Heidelberg, Germany [23]. The storage ring consists of an octagon-shaped ion orbit surrounded by an ultra-high-vacuum chamber of 55.4 m circumference with a base pressure of $\sim 10^{-11}$ mbar, providing a clean environment for electron collision experiments. Dipole and quadrupole magnets direct the ions on their revolving course inside the vacuum tube.

Two independent cold electron beam facilities are located in two of the straight sections of the storage ring. Both of them were used for the present work. The first one (the electron cooler) is equipped with a thermal cathode limiting the transverse electron temperature to ~12.5 meV. In the second one (the electron target [24]) the electrons are extracted from a photocathode [25], thus allowing for much lower electron temperatures. In the present study the parallel and transverse electron temperatures were $kT_{||} \sim 40$ μeV and $kT_{\perp} \sim 1$ meV, respectively.

A strong pilot H_3^+ ion beam was produced from a Penning ion source in order to facilitate the initial setting of the storage-ring magnets. The ions were accelerated to an energy of $E_{\text{beam}} \sim 4.08$ MeV by a radiofrequency quadrupole accelerator (RFQ) followed by an RF linear accelerator and injected into the storage ring. Once all the settings had been optimized, the ion source port was switched to the supersonic expansion source which emitted one ion pulse per injection.

The electron densities in the cooler and target were set to 1.4×10^7 cm^{-3} and 1.34×10^6 cm^{-3}, respectively. The overlap length of the electrons with the ion beam in the electron cooler amounts to ~1.5 m while the electron target length is ~1.1 m. This exposes the ions to electron cooling for an effective fraction of $\eta_c \sim 2.7\%$ of the 55.4 m storage-ring circumference in the electron cooler, and $\eta_t \sim 2.0\%$ in the electron target. The voltage required to match the velocity of the electron target beam to the ion beam (cooling voltage) was $V_{\text{cool}} = 740.9$ V.

After injection into the storage ring the ions are merged with the velocity-matched electron beams of both the electron cooler and the electron target for a 2 s-long precooling period. In this phase the translational temperature of the ions is reduced dramatically in interactions with the mono-energetic electrons and the diameter of the stored ion beam shrinks to ~1 mm. After precooling, the energy of the electron target beam is scanned over the desired collision energy range while the electron cooler stays at the initial cooling energy. During the measurements the electron target energy is "wobbled" repeatedly in cycles consisting of three steps with lengths of 40, 40, and 80 ms, respectively. For the first step—the so-called cooling step—the beam is set to the nominal cooling energy in order to avoid beam dragging effects. The second step is the measurement step. Here the energy is changed for each injection, according to the desired scanning region. The final step is called the reference step. This step is included as a cross-check and for normalization. The energy in this step is set to a value where the spectrum is believed to be independent of the internal energy of the ions and where the cross section exhibits no sharp features. For the present experiment the reference energy was held at a center-of-mass collision energy of 11.5 eV for all runs, corresponding to the maximum of the broad direct DR peak at higher energies. Between each of the wobble steps a 5-ms delay is enforced before the data taking commences in order to make sure that the power supplies have reached their designated values. The ion beam is kept inside the storage ring for a total of ~10 s before it is removed by kicker magnets and the next ion pulse is injected.

1. Rate coefficient measurements

For rate coefficient measurements the neutral fragments resulting from the recombination process are counted by a Si surface barrier detector located ~12 m downstream of the electron target. The detector has an area of 10×10 cm^2 and the beam energy was chosen such that all neutral particles resulting from DR hit the detector, even for the most extreme momentum sharing possible. Neutral events for which an energy equivalent to three atomic mass units is deposited in the detector are counted as DR events. The measured rate R_{DR} is proportional to the DR rate coefficient α, the electron density n_e, and the number of ions in the interaction region N_i,

$$R_{\text{DR}} \propto \alpha n_e N_i. \tag{2}$$

Test measurements without the electron beam show that the number of mass 3 events produced by dissociative charge transfer in collisions with residual gas atoms and molecules is negligible. On the other hand, interactions with residual gas *do* lead to collision-induced dissociation (CID) of H_3^+, resulting in either neutral H or H_2 fragments and events with correspondingly lower energies deposited in the detector. The rate of these events R_{CID} is proportional to the ion current and the residual gas pressure. We use the CID rate during the cooling step as a measure of the ion current to normalize the energy bins within one run of data taking (typically 1–2h). The proportionality between the CID rate and the ion current is warranted, as long as the residual gas pressure does not change significantly. The pressure at various locations in the storage ring is monitored and recorded continuously for verification.

In order to average the data from separate runs taken at different times we cannot rely on constant pressure, however. Therefore, the DR rate at the reference energy step of 11.5 eV is used to normalize and co-add the data from individual runs. Substituting the number of ions N_i by R_{CID} we can express the relative DR rate coefficient as a function of the electron-ion center-of-mass collision energy by

$$\alpha_{\mathrm{rel}}(E_{\mathrm{c.m.}}) = \frac{R_{\mathrm{DR}}(E_{\mathrm{c.m.}})}{n_e(E_{\mathrm{c.m.}})R_{\mathrm{CID}}(E_{\mathrm{beam}})}. \quad (3)$$

The electron density $n_e(E_{\mathrm{c.m.}})$ can be derived from the electron beam current measured in the electron target. To normalize the rate coefficient measurement on an absolute scale we have calibrated the absolute rate coefficient for velocity-matched ion and electron target beams (corresponding to $E_{\mathrm{c.m.}} \sim 0$). These results will be presented in Sec. IV B.

2. *Imaging measurements*

We have performed two-dimensional (2D) DR fragment imaging studies to determine the internal energy of the stored H_3^+ ions. A microchannel plate (MCP) detector is used in combination with a phosphor screen and a CCD camera to measure the relative distance of particle impacts. The imaging detector is located in the straight section downstream of the electron target at a distance of 12.24 m from the center of the target. Only the three-body decay of H_3^+ was considered here, as the outgoing ground-state H atoms in this case have no internal excitation, which greatly simplifies the analysis. For H_3^+ in the rovibrational ground state ~4.8 eV of kinetic energy are released in the three-body DR process. This kinetic energy release is transformed into particle distances of millimeters to centimeters at the end of the ~12 m flight path to the detector. We record the two-dimensional impact distances at the detector for one DR event at a time. By comparing the measured distance distribution with simulated distributions assuming different degrees of rotational excitation, we can infer the average rotational energy stored in the H_3^+ molecules prior to the DR process. The DR fragment imaging method has been used extensively in the past [9,26–28], however, recently we tried to extend the technique to lower rotational temperatures (see, e.g. [29]). For H_3^+ this ultimately leads to a situation where the temperature derivation is limited by the uncertainty in the H_3^+ binding energy. A detailed description of the temperature analysis can be found in Sec. IV A.

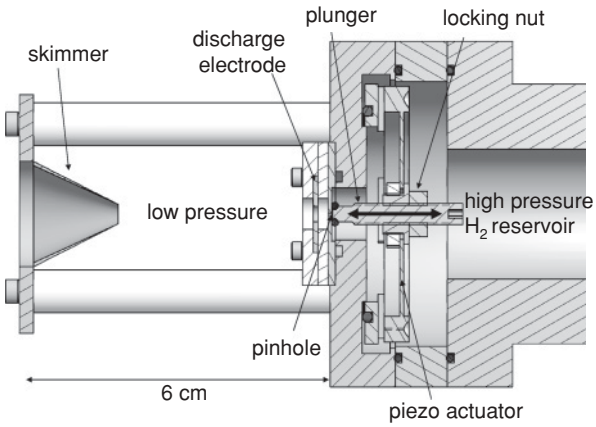

FIG. 1. Schematic of the supersonic expansion ion source. For the spectroscopy measurements, the laser beam crossed between the nozzle and the skimmer, at a distance of ~1 cm upstream of the skimmer.

For the imaging measurements, the electron beam of the target remained velocity matched with the ion beam during the entire storage time. The effect of the electron beam of the cooler on the internal temperature of the H_3^+ ions was investigated through measurements with the cooler turned on and with the cooler turned off.

B. Supersonic expansion source and spectroscopy setup

Schematics of the supersonic expansion source are given in Fig. 1. A piezoelectric actuator valve is used to produce short gas pulses from a high-pressure reservoir into a low-pressure vacuum chamber. The valve design follows the description given by Proch and Trickl [30]. We have added a stainless steel ring in front of the nozzle that serves as a discharge electrode. The piezo is activated by 300 μs-long pulses of −400 V. By applying a potential of −900 V a discharge is initiated between the electrode and the nozzle. The discharge pulse has a length of 1 ms. The gas pulse is delayed with respect to the discharge pulse by 200 μs, hence the gas pulse is embedded in the discharge pulse. Spectroscopic measurements of the rotational temperature of H_3^+ with this source showed no difference for variations of the length and delay of the gas pulse or the order with which the pulses are applied. For the TSR measurements we used backing pressures of 2 bar and either pure n-H_2 or mixtures of argon with n-H_2 and p-H_2, respectively.

The ion source was characterized spectroscopically at the University of Illinois. For this purpose it was connected to a vacuum chamber evacuated to a base pressure of 10 mtorr by a Leybold WS-2001 roots blower backed by a rotary vane pump. The spectroscopy setup is similar to the one described in [31]. It consists of a continuous wave difference frequency laser (DFG) and a continuous wave cavity ring-down spectrometer. We use the DFG laser to produce tunable infrared light (2.2–4.8 μm) at the wavelength difference between two pump laser beams. We split the output of a Nd:YVO_4 laser at 532 nm (Coherent Verdi V-10) into two beams. The first beam is used to pump a continuous wave dye laser (Coherent 899-29)

using Rhodamine 640 to produce laser light at ~622 nm. The second beam from the Nd:YVO_4 laser is passed through an acousto-optic modulator (AOM) and the first-order output is superimposed with the dye laser beam in a MgO-doped periodically poled $LiNbO_3$ crystal. For the present work the difference frequency generation resulted in ~500 μW of light around ~ 3.67 μm. The wavelength of the DFG light is tuned by tuning the dye laser frequency.

The heart of the cavity ring-down spectrometer is a high-finesse cavity that is made from two high-reflectivity mirrors (~99.98%) which are attached directly to the vacuum chamber. The DFG light is coupled into the cavity through the backside of one of the mirrors. A piezoelectric transducer dithers the mirror, effectively altering the cavity length. When the resonance frequency of the cavity and the DFG laser frequency coincide, power builds up inside the cavity. The light leaking out of the backside of the second mirror is recorded by a liquid-nitrogen cooled InSb detector. Once the observed power level exceeds an adjustable threshold, the AOM is switched off and the light intensity ring-down in the cavity is recorded by a high-speed digitizer. Typical ring-down time constants were on the order of 10 μs.

The ion source was mounted such that the laser cavity probed the ions at a distance around 1 cm upstream of the skimmer. Moving the ion source up or down by several millimeters did not result in a change of the measured temperatures.

To combine a pulsed ion source with a continuous wave cavity ring-down setup, it is necessary to synchronize the source pulses with respect to the ring-down occurences. We used a ring-down prediction scheme similar to the one described in [32]. In addition, we implemented a hardware signal derived from the actual discharge current that allows us to distinguish unambiguously between events where the ring-down occurred during a source pulse and ring-downs without ion sample present.

III. SPECTROSCOPIC CHARACTERIZATION OF THE SUPERSONIC ION SOURCE

To characterize the rotational temperature and nuclear spin distribution of the H_3^+ ions produced by the supersonic expansion source, we have measured transitions starting from the five lowest-lying rotational levels to the bending mode fundamental band $(v_1, v_2^l) = (0, 1^1)$. Figure 2 shows the observed transitions and the corresponding energy levels. A review on H_3^+ spectroscopy and notation can be found in [33]. Figure 3 shows a Boltzmann plot for all five transitions measured with a gas mixture of 1:5 n-H_2:Ar at 2 bar. The plot shows that the rotational levels can be fitted very well with a thermal distribution at a temperature of (180 ± 10) K. The level populations observed in pure n-H_2 (no argon admixture) are equally well fit with a thermal distribution, however, they result in a significantly lower temperature of (120 ± 10) K. Although the addition of argon increases the rotational temperature observed at the ion source, the argon-diluted gas mixtures were used for the storage-ring measurements in order to determine the difference in the rate coefficient between o-H_3^+ and p-H_3^+. As the para-hydrogen generator that was used for the DR measurements was not

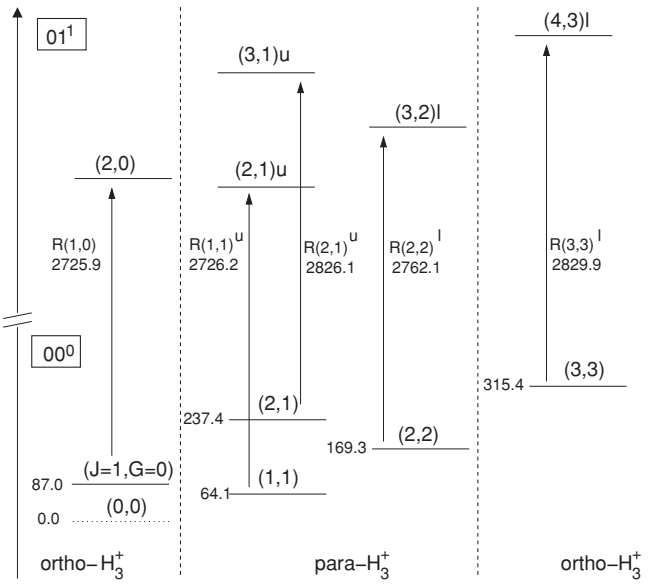

FIG. 2. Diagram of the H_3^+ levels and transitions that were probed for the characterization of the supersonic expansion source. The numbers in parentheses denote the level and transitions labels. The small numeric labels at the left-hand side of the individual levels give the level energy with respect to the symmetry-forbidden rotational ground state ($J = 0, G = 0$) of H_3^+ (plotted as a dotted line). Likewise the transition frequencies are given below the transition labels. All energies and frequencies are in cm^{-1}.

able to provide high enough p-H_2 pressure for pure hydrogen expansions, the gas had to be diluted with argon.

Figure 4 compares the $(1,0)$, $(1,1)^u$, and $(2,2)^l$ lines observed in 1:5 n-H_2:Ar and 1:5 p-H_2:Ar mixtures. Since comparative measurements using n-H_2:Ar and p-H_2:Ar mixtures were rather time-consuming, routinely only three lines were measured. Special care was taken to ensure that the spectra were taken under the same source conditions, with the only change being the nuclear spin mixtures of the precursor gas. The p-H_2 used for the spectroscopy measurements

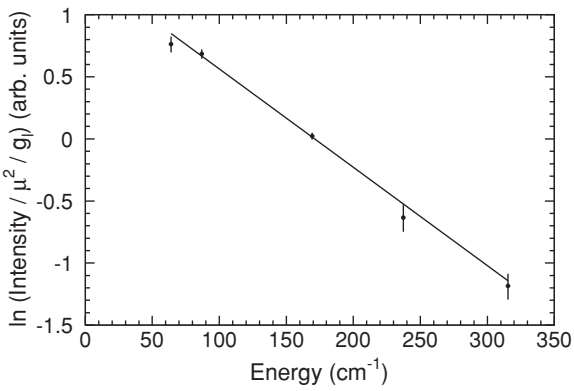

FIG. 3. Boltzmann plot derived from transitions starting at the five lowest-lying rotational levels of H_3^+ observed with the supersonic expansion source at a backing pressure of 2 bar. The gas mixture was 1:5 n-H_2:Ar. The fit results in a temperature of (180 ± 10) K. The transition intensities have been divided by the transition dipole moment μ^2 as given in [35] and by the multiplicity of the lower level g_l.

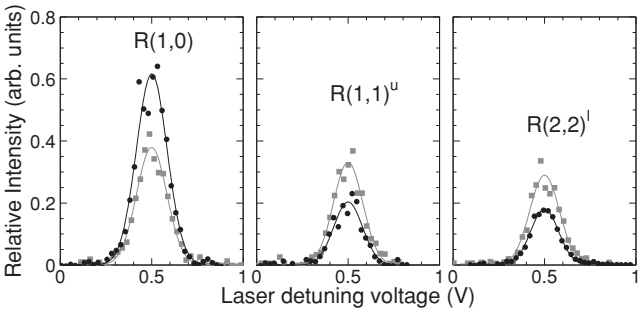

FIG. 4. Comparison of transitions starting from the three lowest rotational levels of H_3^+ measured in the supersonic expansion source with a 1:5 n-H_2:Ar gas mixture (black dots) and a 1:5 p-H_2:Ar gas mixture (gray squares). Calculating the rotational temperature from the two para-lines [R(1,1)^u and R(2,2)^l] results in rotational temperatures of (204 ± 30) K for the n-H_2 mixture and (200 ± 30) K for the p-H_2 mixture. The p-H_3^+ fraction is (47.9 ± 2)% for the n-H_2 mixture and (70.8 ± 2)% for the p-H_2 mixture.

was produced by a dedicated para-hydrogen converter [34] that was calibrated by nuclear magnetic resonance (NMR) measurements. The p-H_2 had a purity of >99%. The relative line strengths of the two para-lines $(1,1)^u$ and $(2,2)^l$ indicates a rotational temperature of (205 ± 30) K in the n-H_2:Ar mixture and (201 ± 30) K in the p-H_2:Ar mixture, respectively. These temperatures are slightly higher than those derived from the fit of the Boltzmann plot, but both methods agree within the uncertainties. Comparison to the intensity of the (1,0) ortho-line allows us to calculate the p-H_3^+ fraction which is (47.9 ± 2)% for the n-H_2:Ar mixture and (70.8 ± 2)% for the p-H_2:Ar mixture, respectively.

It has been shown that vibrational excitations of H_3^+ decay within 2 s of storage [8] and will therefore not survive the precooling phase in storage-ring experiments. On the other hand, the decay of these states could repopulate rotational excitations in steps of $\Delta J = \pm 1$ and thus alter the observed temperatures in the first seconds of storage. In order to constrain the vibrational excitation produced by the ion source, we have carried out a search for the R(1,1) $02^2 \leftarrow 01^1$ transition which has a transition dipole moment that is comparable to the fundamental band. We tried to find the R(1,1) $02^2 \leftarrow 01^1$ line in both pure p-H_2 gas and in a 1:5 p-H_2:Ar mixture, with no success. From the nondetection of this line we establish an upper limit for the fraction of vibrationally excited H_3^+ ions of <2% in the case of pure hydrogen precursor gas—assuming that the rotational excitation would be thermalized in the vibrationally excited levels. The absence of vibrationally excited states seems surprising at first glance, since vibrational excitations typically are cooled much less efficiently by inelastic collisions in supersonic expansion sources, compared to translational and rotational degrees of freedom. The case of H_3^+ may be special, however, since here every collision with a neutral H_2 molecule must be regarded as a chemical reaction, which can lead to proton-hop reactions or even total scrambling of the nuclei. As the H_3^+ molecules undergo many collisions with H_2 during the expansion process, the outcome of this chemical reaction may dominate the excitation pattern rather than inelastic collisions or the vibrational level spacing.

IV. STORAGE-RING RESULTS

A. H_3^+ rotational energy by DR fragment imaging

We have used the kinetic energy release (KER) that is set free in the three-body DR channel to infer the internal excitation of the stored H_3^+ ions inside the storage ring. The amount of energy released for ground-state H_3^+ molecules at zero center-of-mass collision energy can be derived by consideration of the sequence,

$$\begin{aligned} H_3^+ + e &\xrightarrow{-E_b(H_3^+)} H_2 + H^+ + e, \\ H_2 + H^+ + e &\xrightarrow{-E_b(H_2)} H + H + H^+ + e, \\ H + H + H^+ + e &\xrightarrow{+I_p(H)} H + H + H, \end{aligned} \tag{4}$$

where $E_b(H_3^+)$ denotes the binding energy of H_3^+, $E_b(H_2)$ the binding energy of the hydrogen molecule, and $I_p(H)$ the ionization potential of the hydrogen atom. The expected KER for ground-state H_3^+ thus can be calculated as

$$E_{\mathrm{KER}} = I_p(H) - E_b(H_2) - E_b(H_3^+). \tag{5}$$

The hydrogen ionization potential $I_p(H) = 13.5984$ eV [36] and the H_2 binding energy $E_b(H_2) = 4.4781$ eV [37] have been determined with high precision, while the binding energy of H_3^+ is not known as precisely as the other parameters. The experiment of Cosby and Helm [38] resulted in a binding energy of (4.373 ± 0.021) eV. Increasingly accurate theoretical calculations, however, disagree with this value and converge at 4.3300 eV (see, e.g. [39] for an overview). Furthermore, more recent photodissociation data [40] indicate a somewhat lower value of 4.337 eV for the H_3^+ binding energy [41], closer to the theoretical results. Based on the accuracy that calculations of the H_3^+ potential surface have reached and the agreement among the published values, we use the theoretical value as our reference. The expected kinetic energy release for three-body DR from the $(J = 1, G = 1)$ ground state is $E_{\mathrm{KER}} = 4.7903$ eV.

For the temperature analysis we use the sum of the transverse interparticle distances $R^2 = R_1^2 + R_2^2 + R_3^2$ measured by the imaging detector. As the relative distances R_i are proportional to the relative transverse velocities $v_i^\perp$, R^2 is proportional to the total transverse kinetic energy release $E_{\mathrm{KER}}^\perp$,

$$E_{\mathrm{KER}}^\perp = \frac{1}{3\,s^2} E_{\mathrm{beam}} R^2, \tag{6}$$

with s being the flight distance to the detector. To infer the amount of excess energy, we compare the measured distributions of $E_{\mathrm{KER}}^\perp$ to a Monte Carlo simulation of the dissociation process assuming various degrees of internal excitation. In order to simulate the expected distances at the detector precisely, the ion beam energy has to be known to better than 0.5%. Since electron cooling leads to a near-perfect match between the velocities of the electron and ion beams, we use the well-defined velocity of the electrons in the electron target to obtain the energy of the ion beam in the laboratory frame, which results in $E_{\mathrm{beam}} = (4.0784 \pm 0.0017)$ MeV. The simulation includes the effective target overlap length and the dissociation anisotropy as determined in previous measurements [42]. We assume Boltzmann distributions for the rotational excitations in the simulation, which allows us

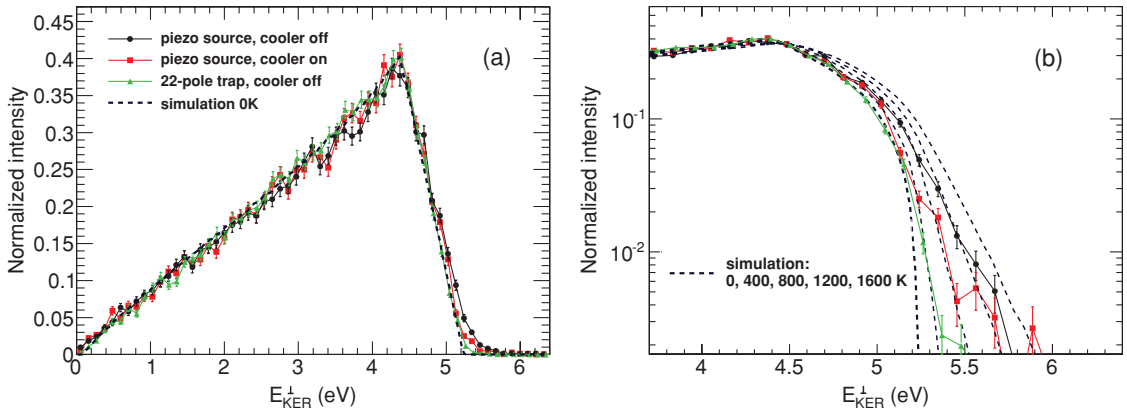

FIG. 5. (Color online) Transverse kinetic energy release distributions resulting from DR fragment imaging measurements. In (a) the measured distributions taken with the piezo expansion source and the electron cooler off are shown as black dots. The supersonic expansion data measured with the electron cooler on are plotted as red squares. Also shown are the results obtained with a cryogenic 22-pole ion injector (green triangles) taken with the electron cooler off. The dashed line represents the simulated distribution for 0 K rotational temperature. In (b) the higher energy region of the same experimental distributions is plotted on a logarithmic scale. Here, the dashed lines represent simulations with (from left to right) 0 K, 400 K, 800 K, 1200 K, and 1600 K rotational temperature. For the data plotted here 1:5 p-H_2:Ar was used as a precursor gas for the supersonic expansion source and pure p-H_2 for the 22-pole injector.

to assign a temperature to each individual simulation run. This choice is motivated by simplicity rather than an exact knowledge of the underlying populations. Furthermore, in the simulation we also assume that the DR rate coefficient is independent of the rotational state.

Figure 5 shows the measured kinetic energy release derived from the 2D particle distance distributions. Here, we plot experimental data for the present work and, for comparison, a TSR measurement performed with the cryogenic 22-pole ion trap in 2007 for which preliminary results were given in [42,43] and whose full analysis has recently been completed [44]. Also plotted are a series of simulated distributions assuming different rotational temperatures. All experimental data plotted in Fig. 5 were obtained using p-H_2 (1:5 p-H_2:Ar in the case of the expansion source) as a precursor gas. The transverse kinetic energy distributions measured using n-H_2 did not show a significant difference in temperatures.

Regarding Figs. 5(a) and 5(b), it is important to note that a visual comparison between experiment and theory becomes most meaningful when it is not done at the tails of the distributions where the statistics are poor. The statistically significant portion of the distribution lies at transverse kinetic energies of <5.2 eV. The fact that the extreme tails of the distributions seem to indicate higher rotational temperatures implies that the population of rotational states is probably not thermal.

We have derived temperature estimates for the respective experimental data sets by minimizing the χ^2 between the experimental and the simulated distributions using the rotational temperature in the simulation as a free parameter. With this method the supersonic expansion data (with the electron beam in the electron cooler being switched off) are best approximated by a simulation with (950 ± 100) K rotational temperature. The quoted uncertainty estimate corresponds to a 90% confidence level for the fit. When the high-density beam of the electron cooler is used in combination with the electron target, the internal temperature of the H_3^+ ions drops significantly to (450 ± 100) K. This electron-induced rotational cooling effect can be seen as a consequence of the tenfold higher electron density present in the electron cooler than in the electron target. The effect has been observed previously for the dissociative recombination of D_2H^+ [45] and can be either assigned to collisional cooling by superelastic electron collisions or to selective depletion of highly excited states in collisions with electrons. It has also been observed for HD^+ ions [29] where it could be clearly assigned to collisional cooling by superelastic electron collisions.

While the 22-pole measurement appears colder than the supersonic expansion data [Fig. 5(b)], it is difficult to get a temperature estimate as there is no significant difference in the χ^2 for simulations with rotational temperatures <300 K [44]. For this measurement the electron cooler beam was switched off after 0.5 s of storage while the electron beam of the electron target interacted with the ions over the whole storage time period.

It should be noted that the imaging results shown here are pushing the technique to its limits. The quoted uncertainties are purely statistical in nature and independent of the approximations that have to be made for the simulation. Furthermore, systematic uncertainties have to be taken into account. For example, a change in the H_3^+ binding energy by 20 meV induces a shift in the simulated curves corresponding to a temperature of $\sim$100 K. An even larger uncertainty is imposed by the determination of the actual overlap length of the electron and ion beams inside the electron target. The uncertainty range of this parameter translates into an uncertainty of $\sim$130 K for the rotational temperature; the length used in the analysis was set as to rather overestimate the derived temperatures within this uncertainty.

The supersonic expansion data reveal a large discrepancy between the spectroscopically determined temperature at the ion source ($\sim$200 K) and the rotational temperature of the stored ions without electron cooling ($\sim$950 K). This difference is indicative of a heating process occurring between ion

production and injection into the storage ring. This heating process is currently not fully understood; however, a possible explanation is given in Sec. V.

For the 22-pole trap measurements the ions were buffer-gas cooled to a nominal temperature of 13 K prior to injection [13,42]. The combined statistical and systematic uncertainties of the imaging method do not permit a definitive statement whether this temperature is maintained throughout acceleration and storage. The deviation of the experimental data from the zero rotational temperature curve at the upper end point of the distribution may also be indicative of a heating process, yielding a small nonthermal population in high-J levels. The above analysis of the 22-pole data applies only for the imaging results which are presented here for comparison of the initial temperatures of the ion sources. Rate coefficient measurements with the 22-pole trap were usually carried out using both electron beams; a discussion of the resulting temperatures and detailed rate coefficient studies will be presented elsewhere [44].

B. Absolute DR rate coefficient measurement

Absolute measurements of the H_3^+ DR rate coefficient were carried out in the CRYRING experiment in 2002 [11]. Subsequent studies at TSR [13] were normalized to these measurements at the high-energy direct DR peak. Recent studies at CRYRING, however, had to be scaled by a factor of 0.65 to be brought into agreement with the 2002 data [22]. To calibrate the absolute scale of the rate coefficient independently, we have analyzed lifetime measurements of the stored ion beam with and without the electron target beam (a similar method has been used in [46]). Figure 6 shows a plot of the intensity of the stored H_3^+ beam as a function of the storage time, as measured with a scintillation detector situated in the dipole magnet chamber downstream of the electron target. The events recorded in this detector correspond to charged particles resulting from interactions of the H_3^+ beam with the residual gas. For the measurement shown in Fig. 6 the electron target beam was set to the nominal cooling energy ($E_{\text{c.m.}} \sim 0$) initially and after 12 s of storage it was switched off. The electron cooler beam remained off for

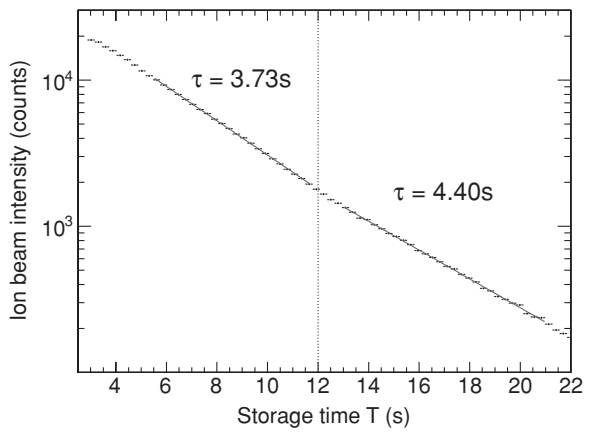

FIG. 6. Plot of the intensity of the H_3^+ ion beam as a function of the storage time. For the first 12 s of storage the electron target beam is switched on and set to the nominal cooling energy. At a storage time of $T = 12$ s the electron beam is switched off.

the entire lifetime measurement. The decay curve at storage times $T > 12$ s is fitted by an exponential decay with a decay constant $\tau_{\text{off}} = 4.40$ s. We attribute this decay to an effective loss rate inflicted by residual gas and described by

$$R_{\text{eff}}^{\text{res}} = \frac{1}{\tau_{\text{off}}}. \tag{7}$$

At storage times smaller than 12 s, the decay is due to both residual gas and electron interactions in the electron target. It can be fitted by an exponential decay with $\tau_{\text{on}} = 3.73$ s. Assuming that the dominating loss process induced by the electron target beam is DR, we can write

$$R_{\text{eff}}^{\text{res}} + R_{\text{DR}} = \frac{1}{\tau_{\text{on}}}. \tag{8}$$

Substituting Eq. (7) in Eq. (8) and solving for R_{DR} yields

$$R_{\text{DR}} = \frac{1}{\tau_{\text{on}}} - \frac{1}{\tau_{\text{off}}}, \tag{9}$$

which can be converted into the DR rate coefficient by

$$\alpha_{\text{DR}} = \frac{1}{n_e \eta_t}\left(\frac{1}{\tau_{\text{on}}} - \frac{1}{\tau_{\text{off}}}\right), \tag{10}$$

where n_e denotes the electron density in the target overlap region and η_t the ratio of the effective electron target length and the storage-ring circumference. With $n_e = 1.34 \times 10^6$ cm^{-3} and $\eta_t = 0.0199$ we calculate an H_3^+ DR rate coefficient of $\alpha_{\text{DR}} = 1.53 \times 10^{-6}$ cm^3 s^{-1} at cooling energy. Note that this value is used to calibrate the measured rate coefficient before corrections for the toroidal regions of the electron target are applied. The toroid correction procedure [47] then accounts for the effective target length much more precisely and makes the final result almost independent of the exact value of η_t. We estimate an uncertainty of 30% for the calibration method of the absolute scale described above.

Figure 7 shows a comparison of the rate coefficient from the present work (1:5 n-H_2:Ar mixture) normalized to the lifetime measurement, and the 2002 CRYRING data. For the present work the electron cooler was switched on during the measurement and set to zero center-of-mass collision energy, while the electron target energy was scanned as described in Sec. II A 1. The comparison shows that the rate coefficient measured with the piezo expansion source and n-H_2:Ar is practically identical on an absolute scale with the rate coefficient measured at CRYRING with n-H_2 and a similar type of ion source. The fact that the rate coefficient can be reproduced in such detail at a different storage ring with different beam energies and measurement schemes confirms the stability and reproducibility of the storage-ring technique.

C. Dependence of the DR rate coefficient on the nuclear spin

To examine the dependence of the DR rate coefficient on the nuclear spin of H_3^+, we carried out measurements utilizing the supersonic expansion source with n-H_2:Ar and p-H_2:Ar gas mixtures, respectively. At center-of-mass collision energies >0.3 eV the measured rate showed no dependence on the nuclear spin of the precursor gas, in agreement with previous experiments [13,22]. In the following, we focus on the low energy region.

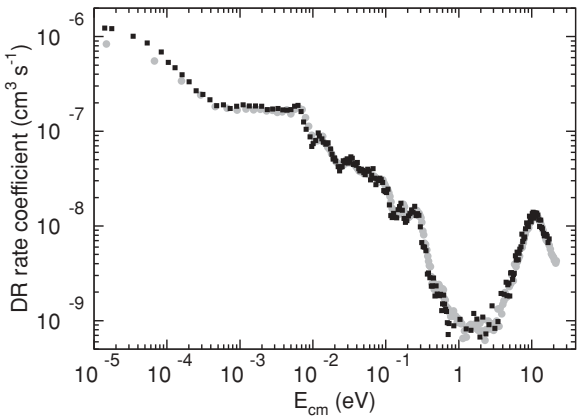

FIG. 7. DR rate coefficient as a function of the center-of-mass collision energy $E_{\text{c.m.}}$. The black squares depict the results of the present measurement obtained using the supersonic expansion source with a 1:5 n-H_2:Ar gas mixture. The data are independently normalized to the absolute rate measurement described in Sec. IV B. The gray dots represent the 2002 CRYRING measurement [11].

Figure 8(a) shows a comparison of the rate coefficient at low energies obtained with 1:5 n-H_2:Ar and 1:5 p-H_2:Ar mixtures, respectively. The rate coefficient has been multiplied by $\sqrt{E_{\text{c.m.}}}$ in all cases to eliminate the inherent $1/v$ dependence for clarity of presentation. The data obtained using p-H_2 show a slightly higher rate coefficient at low collision energies. While this general trend is consistent with previous measurements, we observe structural details in the rate coefficients that were not visible in either of the previous studies. The higher

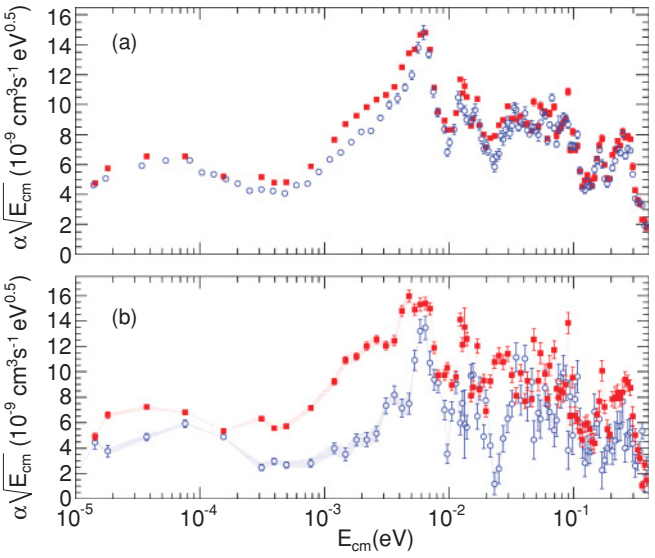

FIG. 8. (Color online) Comparison of the DR rate coefficient for different nuclear spin modifications of H_3^+. The upper panel (a) shows the results obtained with the supersonic expansion source and 1:5 n-H_2:Ar (blue circles) and 1:5 p-H_2:Ar (red squares) mixtures. The lower panel (b) shows the extrapolated results for "pure" p-H_3^+ (red squares) and "pure" o-H_3^+ (blue circles). For the extrapolation we assume a p-H_3^+ fraction of $(47.9 \pm 2)\%$ for n-H_2:Ar and $(70.8 \pm 2)\%$ for p-H_2:Ar (see discussion in the text). The error bands in the lower panel represent the effect of the 2% uncertainty in the spectroscopic determination of the p-H_3^+ fractions.

transverse electron temperature of ~4 meV in the experiment of Kreckel *et al.* [13] and ~2 meV for Tom *et al.* [22], as compared to ~1 meV for the present work, might be partly responsible for the absence of structure in those measurements. On the other hand, the 2002 CRYRING measurements [11] that were performed with the same ~2 meV transverse electron temperature as those of Tom *et al.* display distinctly more structure at low energy. Tom *et al.* suggest that the presence of excited rotational states, perhaps due to residual gas collisions in CRYRING, might have smoothed out the rate coefficient curve [22].

Figure 8(b) shows the rate coefficients of o-H_3^+ and p-H_3^+ extrapolated from the present measurements using n-H_2:Ar and p-H_2:Ar mixtures. For the extrapolation we assumed that the n-H_2:Ar mixture results in a p-H_3^+ fraction of 47.9% and the p-H_2:Ar mixture results in a p-H_3^+ fraction of 70.8%, as inferred from the cavity ring-down spectra. This procedure can be questioned, since the rotational temperature derived from DR fragment imaging is much higher than the rotational temperature of the ion source in the spectroscopic measurements. Hence, a heating process must exist that changes the rotational level populations. It is not clear whether this process will also influence the p-H_3^+ fraction, but since the initial 200 K temperature of the ion source is not too far from room temperature, here we assume that the measured nuclear spin distribution is a result of the high-temperature equilibrium as established in H_3^+-H_2 collisions and that further collisions with the same buffer gas at higher collision energies will not alter the p-H_3^+ fraction.

It should be mentioned, however, that experiments with isotopically substituted species suggest that $H_3^+ + H_2$ collisions at increased temperatures [48] proceed predominantly via the proton-hop channel. As the proton-hop reaction favors para-enrichment of H_3^+ in p-H_2 gas (see [49,50] for nuclear spin selection rules in $H_3^+ + H_2$ collisions), this could lead to an increase of the p-H_3^+ fractions when the ions are extracted through p-H_2 gas in the present case. Effectively, this would lead us to overestimate the differences between the o-H_3^+ and p-H_3^+ rate coefficients extrapolated for Fig. 8(b).

With that being said, the comparison in Fig. 8(b) shows differences between the rate coefficients for o-H_3^+ and p-H_3^+ at narrow structures in their energy dependence. At energies between 10^{-3} eV and 5×10^{-3} eV the p-H_3^+ rate coefficient is higher than the o-H_3^+ rate coefficient by roughly a factor of two. Below 10^{-3} eV the results must be considered less informative as the transverse electron temperature will dominate the measured rates. Above 10^{-2} eV there are distinct regions where the rate coefficients for the two nuclear spin modifications exhibit counterpropagating trends, resulting in rather large differences in the rate coefficients. Most notably is the region around 2.5×10^{-2} eV where the o-H_3^+ rate coefficient almost tends toward zero. Comparison to theory will reveal whether these energies can be matched with resonances in the DR cross section.

V. ION EXTRACTION

The fragment imaging results confront us with the fact that the rotational temperatures of the stored H_3^+ ions are much higher than the spectroscopically measured temperatures. On

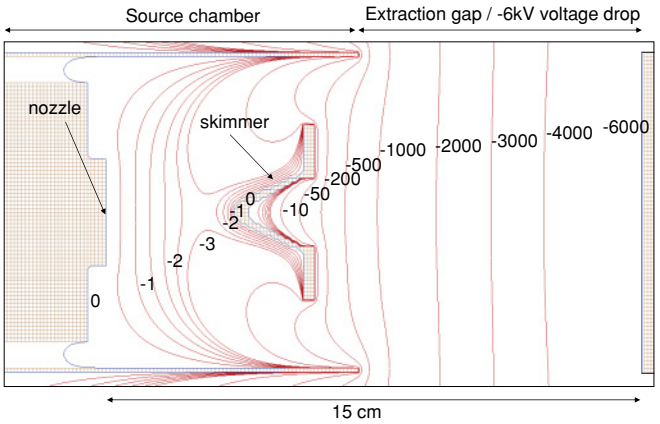

FIG. 9. (Color online) SIMION simulation of the extraction region for the supersonic ion source. The equipotential lines show the voltage difference with respect to the nozzle unit (in volt).

the other hand, the temperature of the stored ions *does* depend on the ion source that is used, which signifies that we are not dealing with a universal heating process inside the storage ring. Therefore, the acceleration process that takes place between the ion formation in the ion source and the DR measurements is the primary suspect for inducing rotational heating.

We have simulated the electric fields in the acceleration region for the supersonic expansion ion source with the SIMION 3D program suite [51,52]. Prior to injection into the accelerator of the TSR facility, the ions are extracted from the source and preaccelerated to 12 keV in two steps of 6 kV. Figure 9 shows the equipotential lines for the first extraction stage. It can be seen that besides the intended potential drop between the skimmer and the extraction electrode, the field lines also penetrate slightly into the region between skimmer and nozzle where the pressure is still high. Potentials up to 3 eV are reached in this region, possibly disturbing the expansion process.

Figure 10 shows various parameters in the region downstream of the nozzle for a pure hydrogen expansion. The upper panel shows the H_2 number density $n(H_2)$ on the axis going through the midpoint of the nozzle and the center of the skimmer. The number density was estimated using a simple $1/r^2$ scaling law [53]. The middle panel shows the electric field strength and the lower panel the estimated mean free path d of the H_3^+ ions. The mean free path is calculated using the following assumptions: (i) the rate coefficient for $H_3^+ + H_2$ collisions is constant with a value $\alpha_{\mathrm{col}} = 1.3 \times 10^{-9}$ cm^3 s^{-1} [54]; (ii) the energy and thus the velocity $v(H_3^+)$ of the H_3^+ ions is determined by the electrostatic potential alone. With these assumptions the energy-dependent collision cross section can be approximated by

$$\sigma_{\mathrm{col}} = \frac{\alpha_{\mathrm{col}}}{v(H_3^+)}, \tag{11}$$

and the mean free path is given by

$$d = \frac{1}{\sigma n(H_2)}. \tag{12}$$

The plots show that the ions are likely to undergo many collisions while being accelerated away from the nozzle. The skimmer extends from distances of ~3.7 cm to ~5.7 cm after

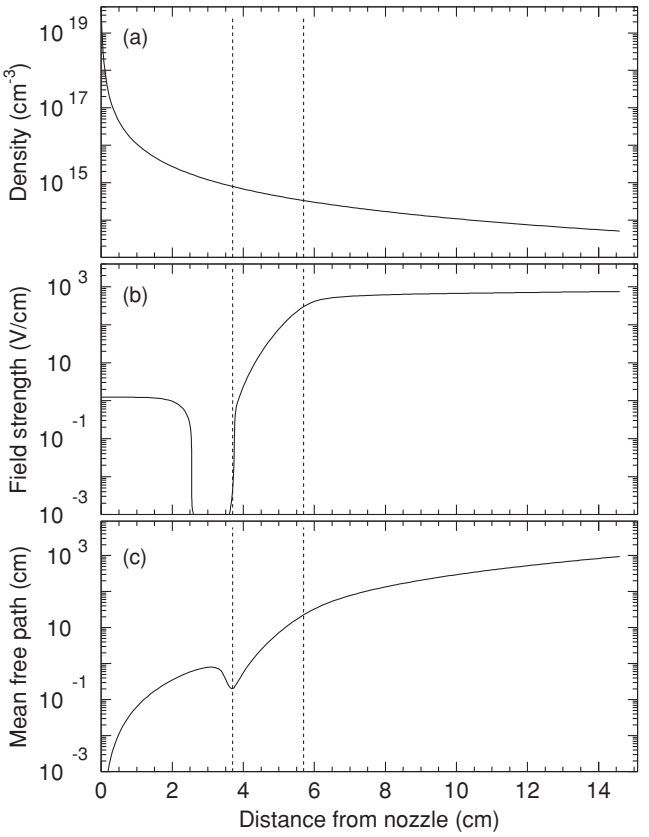

FIG. 10. Plots of the density (a), electric field strength (b), and the estimated mean free path (c) in the extraction region of the supersonic expansion source for pure H_2 gas. Details on the mean free path approximation are given in the text. The dashed lines mark the beginning and the end of the skimmer.

the nozzle. The mean free path in this region ranges from 10^{-3} cm to 1 cm, while electric field strengths are on the order of 0.1 V/cm. This indicates that the ions undergo many collisions while being accelerated through the gas before they reach the skimmer. After the skimmer the mean free path increases but the ions are still likely to interact with the expanding gas. It is possible that these nonthermal collisions are responsible for the elevated temperatures observed in the DR measurements. In order to avoid collisions during the ion extraction a longer undisturbed flight path before acceleration would be required.

VI. SUMMARY AND PERSPECTIVES

We have performed high-resolution measurements of the dissociative recombination of H_3^+ utilizing a spectroscopically calibrated supersonic expansion source. The line intensities obtained by cavity ring-down spectroscopy at the ion source indicate a rotational temperature of ~200 K with 1:5 H_2:Ar gas mixtures. A comparison of the rate coefficient obtained using n-H_2 to a previous DR experiment with a similar type of ion source at CRYRING [11] shows a very strong agreement.

Measurements with n-H_2 and p-H_2 precursor gas show detailed differences in the rate coefficients for o-H_3^+ and p-H_3^+ at low energies.

While the spectroscopic measurements with the piezo ion source result in rotational temperatures on the order of 200 K, fragment imaging of the stored ions inside the storage ring reveal temperatures around ~950 K and ~450 K, respectively, where the lower value is reached during the interaction with cold electrons at the elevated density of the electron cooler. The large discrepancy between the spectroscopy results and the fragment imaging data is indicative of a heating process between ion production and electron recombination.

The apparent difference in temperature between the 22-pole trap ion source and the supersonic expansion seen in the fragment imaging data suggests that the heating is not a universal property of storage-ring measurements but is more likely to occur during the ion extraction. For future measurements a careful analysis of the electric fields and pressure profile in the ion extraction section is called for.

Previous and present comparisons between different storage rings exhibit a remarkable degree of reproducibilty for H_3^+ as well as for other molecular ions (see, e.g. [55]). The H_3^+ DR rate coefficient has been measured at heavy-ion storage rings with a multitude of different ion sources, ranging in temperature between 10 and 4000 K; still the rate coefficient never changed by more than 40%. The work presented here shows, however, that in order to reliably determine the rotational temperature of the stored ions, it has to be measured *in situ*, inside the storage ring. The fact that previous measurements with supersonic ion sources were done with similar ion extraction geometries and that the rate coefficient obtained in these measurements agrees with the present measurement in all details, suggests that these measurements were affected by the same heating mechanism. Unfortunately, no imaging data exist for these experiments to determine the rotational temperature.

Additional studies with optimized extraction geometries to reach lower rotational temperatures, as well as measurement schemes that would allow for a direct spectroscopic determination of the populated H_3^+ rotational levels inside the storage ring [56], are foreseen in the near future.

ACKNOWLEDGMENTS

H.K., K.N.C., B.A.T., and B.J.M. were supported by National Science Foundation (NSF) Grant No. PHY08-55633. O.N. was supported by NSF Astronomy and Astrophysics Grant No. AST-0807436. M.L. was supported by Astronomy and Physics Research and Analysis Grant No. NNX09AF74G. We thank Daniel W. Savin as the principal investigator of both these grants for partial support of the present project. H.B. acknowledges partial support from the German-Israeli Foundation for Scientific Research and Development (G.I.F.) under Grant No. I-900-231.7/2005 and from the European Project ITS LEIF (Grant No. HRPI-CT-2005-026015). We thank P. Buscay for assistance with the mechanical drawings for the supersonic expansion source. We thank M. König and the accelerator staff at MPI-K for their excellent support during the beam time. Support from the Max-Planck Society is acknowledged.

[1] A. Dalgarno, Adv. At. Mol. Opt. Phys. **32**, 57 (1994).
[2] M. Larsson and A. E. Orel, *Dissociative Recombination of Molecular Ions* (University Press, Cambridge, 2008).
[3] N. G. Adams, D. Smith, and E. Alge, J. Chem. Phys. **81**, 1778 (1984).
[4] D. Smith and N. G. Adams, J. Chem. Soc., Faraday Trans. 2 **83**, 149 (1987).
[5] H. H. Michels and R. H. Hobbs, Astrophys. J. Lett. **286**, L27 (1984).
[6] T. Amano, Astrophys. J. Lett. **329**, L121 (1988).
[7] M. Larsson *et al.*, Phys. Rev. Lett. **70**, 430 (1993).
[8] H. Kreckel *et al.*, Phys. Rev. A **66**, 052509 (2002).
[9] D. Strasser *et al.*, Phys. Rev. Lett. **86**, 779 (2001).
[10] H. Kreckel, J. Tennyson, D. Schwalm, D. Zajfman, and A. Wolf, New J. Phys. **6**, 151 (2004).
[11] B. J. McCall *et al.*, Nature (London) **422**, 500 (2003).
[12] B. J. McCall *et al.*, Phys. Rev. A **70**, 052716 (2004).
[13] H. Kreckel *et al.*, Phys. Rev. Lett. **95**, 263201 (2005).
[14] H. Kreckel, J. Mikosch, R. Wester, J. Glosík, R. Plašil, M. Motsch, D. Gerlich, D. Schwalm, D. Zajfman, and A. Wolf, J. Phys.: Conf. Ser. **4**, 126 (2005).
[15] J. Glosík, I. Korolov, R. Plašil, O. Novotný, T. Kotrík, P. Hlavenka, J. Varju, I. A. Mikhailov, V. Kokoouline, and C. H. Greene, J. Phys. B: At. Mol. Opt. Phys. **41**, 191001 (2008).
[16] J. Glosík, R. Plašil, I. Korolov, T. Kotrík, O. Novotný, P. Hlavenka, P. Dohnal, J. Varju, V. Kokoouline, and C. H. Greene, Phys. Rev. A **79**, 052707 (2009).
[17] S. Datz, G. Sundström, C. Biedermann, L. Broström, H. Danared, S. Mannervik, J. R. Mowat, and M. Larsson, Phys. Rev. Lett. **74**, 896 (1995).
[18] V. Kokoouline, C. H. Greene, and B. D. Esry, Nature (London) **412**, 891 (2001).
[19] V. Kokoouline and C. H. Greene, Phys. Rev. A **68**, 012703 (2003).
[20] V. Kokoouline and C. H. Greene, Phys. Rev. Lett. **90**, 133201 (2003).
[21] S. F. Dos Santos, V. Kokoouline, and C. H. Greene, J. Chem. Phys. **127**, 124309 (2007).
[22] B. A. Tom *et al.*, J. Chem. Phys. **130**, 031101 (2009).
[23] D. Habs *et al.*, Nucl. Instr. Meth. Phys. Res. B **43**, 390 (1989).
[24] F. Sprenger, M. Lestinsky, D. A. Orlov, D. Schwalm, and A. Wolf, Nucl. Instr. Meth. Phys. Res. A **532**, 298 (2004).
[25] D. A. Orlov, U. Weigel, D. Schwalm, A. S. Terekhov, and A. Wolf, Nucl. Instr. Meth. Phys. Res. A **532**, 418 (2004).
[26] D. Strasser, L. Lammich, H. Kreckel, M. Lange, S. Krohn, D. Schwalm, A. Wolf, and D. Zajfman, Phys. Rev. A **69**, 064702 (2004).
[27] D. Zajfman, Z. Amitay, C. Broude, P. Forck, B. Seidel, M. Grieser, D. Habs, D. Schwalm, and A. Wolf, Phys. Rev. Lett. **75**, 814 (1995).
[28] Z. Amitay *et al.*, Science **281**, 75 (1998).
[29] D. Shafir *et al.*, Phys. Rev. Lett. **102**, 223202 (2009).
[30] D. Proch and T. Trickl, Rev. Sci. Instrum. **60**, 713 (1989).

[31] B. A. Tom, A. A. Mills, M. B. Wiczer, K. N. Crabtree, and B. J. McCall, J. Chem. Phys. **132**, 081103 (2010).
[32] P. Birza, T. Motylewski, D. Khoroshev, A. Chirokolave, H. Linnartz, and J. P. Maier, Chem. Phys. **283**, 119 (2002).
[33] C. M. Lindsay and B. J. McCall, J. Mol. Spectrosc. **210**, 60 (2001).
[34] B. A. Tom, S. Bhasker, Y. Miyamoto, T. Momose, and B. J. McCall, Rev. Sci. Instrum. **80**, 016108 (2009).
[35] M. Goto, B. J. McCall, T. R. Geballe, T. Usuda, N. Kobayashi, H. Terada, and T. Oka, Publ. Astron. Soc. Japan **54**, 951 (2002).
[36] W. R. Johnson and G. Soff, At. Data Nucl. Data Tables **33**, 405 (1985).
[37] A. Balakrishnan, V. Smith, and B. P. Stoicheff, Phys. Rev. Lett. **68**, 2149 (1992).
[38] P. C. Cosby and H. Helm, Chem. Phys. Lett. **152**, 71 (1988).
[39] W. Kutzelnigg and R. Jaquet, Phil. Trans. R. Soc. A **364**, 2855 (2006).
[40] U. Galster, P. Kaminski, M. Beckert, H. Helm, and U. Müller, Eur. Phys. J. D **17**, 307 (2001).
[41] H. P. Helm (private communication).
[42] A. Petrignani *et al.*, J. Phys.: Conf. Ser. **192**, 012022 (2009).
[43] H. Kreckel *et al.*, J. Phys.: Conf. Ser. **88**, 012064 (2007).
[44] A. Petrignani *et al.* (in preparation).
[45] L. Lammich *et al.*, Phys. Rev. Lett. **91**, 143201 (2003).
[46] H. B. Pedersen *et al.*, Phys. Rev. A **72**, 012712 (2005).
[47] Z. Amitay, D. Zajfman, P. Forck, U. Hechtfischer, B. Seidel, M. Grieser, D. Habs, R. Repnow, D. Schwalm, and A. Wolf, Phys. Rev. A **54**, 4032 (1996).
[48] D. Gerlich, J. Chem. Soc., Faraday Trans. **89**, 2199 (1993).
[49] M. Cordonnier, D. Uy, R. M. Dickson, K. E. Kerr, Y. Zhang, and T. Oka, J. Chem. Phys. **113**, 3181 (2000).
[50] T. Oka, J. Mol. Spectrosc. **228**, 635 (2004).
[51] Computer code SIMION 3D 8.0, Scientific Instrument Services, Ringoes, NJ, 2008 [http://www.simion.com].
[52] D. A. Dahl, Int. J. Mass Spectrom. **200**, 3 (2000).
[53] H. C. W. Beijerinck, R. J. F. V. Gerwen, E. R. T. Kerstel, J. F. M. Martens, E. J. W. V. Vliembergen, M. r. Th. Smits, and G. H. Kaashoek, Chem. Phys. **96**, 153 (1985).
[54] N. G. Adams and D. Smith, Astrophys. J. **248**, 373 (1981).
[55] A. Al Khalili *et al.*, Phys. Rev. A **68**, 042702 (2003).
[56] A. Petrignani *et al.*, J. Phys.: Conf. Ser. **194**, 022101 (2009).